Hindawi
International Journal of Antennas and Propagation
Volume 2022, Article ID 9724535, 13 pages
https://doi.org/10.1155/2022/9724535

Research Article

Broadband Circularly Polarized Antennas with Compact Radiator Using Characteristic Mode Analysis

Wei Xu, Jingchang Nan, and Jing Liu

School of Electronic and Information Engineering, Liaoning Technical University, Huludao 125100, China

Correspondence should be addressed to Wei Xu; xuwei@lntu.edu.cn

Received 3 January 2022; Revised 29 March 2022; Accepted 18 June 2022; Published 12 July 2022

Academic Editor: Francesco D'Agostino

In this paper, a general design procedure of simple four steps for wideband circularly polarized (CP) antenna based on characteristic mode analysis (CMA) is proposed. CMA is performed to investigate the CP generation principle of the proposed radiator. Modal currents and their corresponding radiation patterns are studied for mode selection and feeding placement to achieve CP operation. Then, two feeding mechanisms are introduced to constitute two CP antenna prototypes, which are further analyzed and optimized by CMA. With the physical insight into radiation characteristics of the prototypes, two antennas employing coplanar waveguide (CPW) as feed are designed and optimized by full-wave simulation. To validate the design procedure, both antennas with the same dimension ($35 \times 40 \times 1.6\,mm^3$) are fabricated and measured. The experimental results show that both of the antennas have good CP radiation performance with a peak gain of 4.0 dBic and 2.5 dBic and axial ratio bandwidth (ARBW) of 48.3% and 44%, respectively. In addition, the experimental results are in good agreement with the radiation information provided by CMA.

1. Introduction

Circularly polarized (CP) antennas have an extensive attraction for modern wireless communication systems. Many works of literature have pointed out that circular polarization has advantages over linear polarization in reducing the multipath effects, polarization mismatches, and Faraday's rotation effects in the ionosphere [1]. The basic requirement for an antenna to radiate CP waves is to excite orthogonal components of equal amplitudes and 90° phase difference, yet in reality, this is challenging to be obtained within broadband.

Numerous approaches to realizing CP antennas have been reported in the literature. An effective technique for achieving a wide axial ratio bandwidth (ARBW) is by employing a 90° power divider [2]. Several alternative techniques have been implemented for CP generation mostly achieved by introducing some symmetric and/or asymmetric perturbations into the antenna. These include CPW-Fed Square Slot with a widened tuning stub [3], two L-grounded strips on opposite corners [4], and asymmetric defective ground [5]. Also perturbations in the form of slot structures [6], feed lines [7], two feed ports [8], and array configurations [9] are widely utilized.

However, antenna geometries of these designs have also indicated that the crux associated with CP radiation is how to optimize the patch shapes and reorganize the two linear polarized modes perpendicular to each other into circular polarization. This procedure is usually accomplished by full-wave simulation and optimization based on engineering experience and intuition with little physical insight.

As an alternative technique, characteristic mode analysis (CMA) possesses attractive features in the design and optimization of antennas [10–12]. The CMA was first formulated by Garbacz in 1968 [13] and later refined by Harrington and Mautz in 1971 [14]. Characteristic modes are current modes that correspond to the eigenvectors of a particular weighted eigenvalue equation involving a generalized impedance matrix of the conductor. Hence, characteristic modes can be used to expand the total current on the conductor surface [15]. There is an eigenvalue or characteristic angle associated with each characteristic mode of an antenna in the absence of excitation [16]. The information about the current distribution and far-field radiation provided by CMA paves the way for enhancing the antenna's performance [17, 18] and providing guidelines for the excitation of antenna designs [19, 20], which leads to a systematic design methodology with physical insight [21–23], in contrast to the quite time-consuming traditional analysis or trial-and-error approaches, which usually bring little physical understanding about the antenna behavior.

Two novel compact broadband CP antennas with the same radiator fed by different CPW networks are proposed, and CMA is employed for designing and optimizing in this paper. The radiator consists of a semicircle and a circular sector of 110°. Utilizing CMA, the radiator is first analyzed, and two pairs of degenerate modes with the potential to generate CP waves are selected for the design of the next step. Feed lines are designed based on different feeding mechanisms, and their placement is studied to excite the desired modes. Then two prototypes of the antenna are further analyzed and optimized by CMA to achieve the optimum geometry and placement of the feed lines. A full-wave EM-driven optimization is subsequently applied to tune the geometrical parameters of the CPW networks, improving both the impedance matching and the ARBW. The electrical characteristics of both antennas indicate that good performance over a wide bandwidth can be easily implemented by CMA. Fabricated antennas experimentally validate the effectiveness of the proposed method and design procedure.

2. Characteristic Mode Analysis for CP Radiation

According to the theory of characteristic mode (TCM) [13, 14], the total current J on the perfect conductor surface can be expressed as a linear superposition of characteristic mode currents J_n:

$$J = \sum_n \alpha_n J_n, \tag{1}$$

where α_n denotes the weighting coefficient (MWC) of the characteristic current J_n and can be calculated by the following:

$$\alpha_n = \frac{V_n^i}{1 + j\lambda_n}, \tag{2}$$

where λ_n are the eigenvalues indicating that the corresponding mode is resonant and radiates the most efficiently as it equals to zero. V_n is the modal excitation coefficient (MEC), which models the coupling between the excitation and the nth mode. It determines whether the corresponding mode is excited by the antenna feed or incident field and can be expressed as follows:

$$V_n = \int J_n \cdot E_i \, \mathrm{d}s. \tag{3}$$

To better measure the resonant frequency and potential contribution to the radiation of a mode, modal significance (MS) is defined.

$$\mathrm{MS} = \left| \frac{1}{1 + j\lambda_n} \right|. \tag{4}$$

MS, with the independence of the external stimulus, is the intrinsic property of each mode. Obviously, the value of MS depends only on the eigenvalues. The mode resonates and radiates the most efficiently as $\mathrm{MS} = 1$. Another important parameter is the characteristic angle (CA), which is more suitable to depict the eigenvalue, especially as the eigenvalue is close to zero or tends to infinity, defined as follows [16]:

$$\mathrm{CA} = 180^\circ - \tan^{-1}(\lambda_n). \tag{5}$$

CA indicates the phase angle lag between the real characteristic current and its associated characteristic field. The most efficient radiation is achieved as CA equals 180°.

Based on the principle of CP radiation, the requirements for these two modes are as follows:

(1) The modal significances are the same $\mathrm{MS}_1 = \mathrm{MS}_2$
(2) The CA difference is 90°: $|\mathrm{CA}_1 - \mathrm{CA}_2| = 90^\circ$
(3) The mode current distributions are orthogonal to each other

Besides, the modal field at the same directivity of interest can ensure a stable radiation pattern in the far-field, generally for the narrowband antenna design with high uniform directivity.

3. The Procedure of CP Generation Based on CMA

A four-step design procedure using characteristic mode theory has been used to design a wideband circular polarized patch antenna. A flowchart detailing the process is shown in Figure 1.

Step 1. CMA is employed to assess the potential of CP radiation for a radiator and optimize geometrical parameters to achieve a wide CP operating band. MS and CA are the first criteria to determine whether the parameter sweep meets the requirements, and then the current distribution of the corresponding modes is analyzed to further confirm that the pair of modes can contribute to CP radiation.

Step 2. According to different design requirements, there are different schemes for mode selection. For example, for the CP antenna design with a stable radiation pattern at $\pm Z$ direction, CP modes radiate in the $\pm Z$ direction are required. For omnidirectional CP radiation, orthogonal omnidirectional modes should be selected. In this design, broadband is pursued at the cost of radiation stability, that is, all CP modes that may contribute to CP radiation are under consideration. Note that the choice based on CMA is to find the maximum possible CP bandwidth and requires further validation.

Step 3. Feeding mechanism is determined based on the modal currents and the optimal feeding positions are

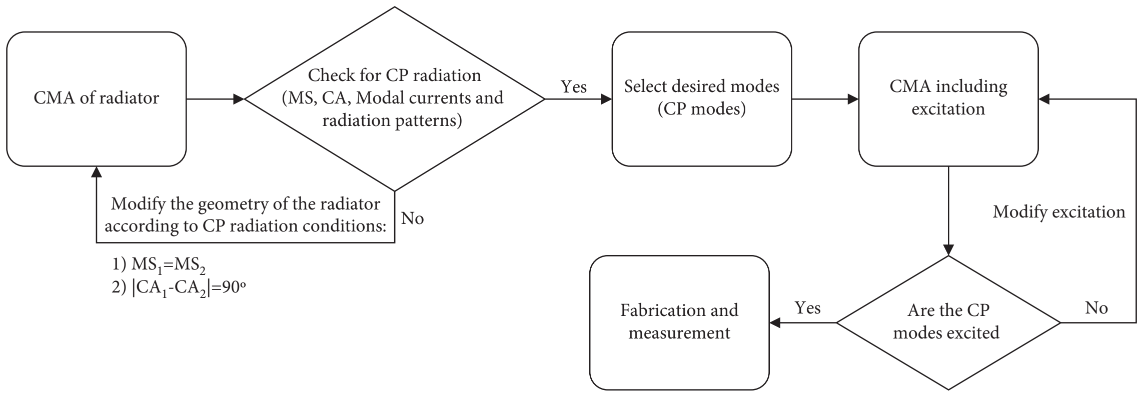

Figure 1: Flowchart outlining design process.

predicted to excite the desired modes. Then, two prototypes of the antenna are proposed, and CMA is performed again for each prototype to optimize the geometrical parameters of the feed line as in Step 2. Then, complete antenna structures are designed and simulated.

Step 4. The proposed antennas are fabricated and measured to validate the design procedure.

3.1. Existing Modes of the Proposed Radiator. The configuration of the radiator is proposed in Figure 2. A semicircle patch and a circular sector of A_c degrees patch overlap with centers apart of d_c printed on an FR-4 substrate ($\epsilon_r = 4.4$ and $H_d = 1.6$ mm), which have the same radius of R. The substrate with no ground is assumed to be loss-free and infinite and the radiation boundary is applied in all directions for CMA. In order to meet the requirements of CP generation, the geometric parameters of the radiator are studied by CMA over the frequency band of 1–8 GHz. For the sake of brevity, the process of parametric analysis is omitted here. The optimized values of R, A_c, and d_c for the radiator are 15 mm, 110°, and 1.2 mm, respectively.

The MS and CA of the first six characteristic modes calculated at 4 GHz are presented in Figure 3. It can be seen that modes J_1 and J_2 have the same MS of 0.73 at around 3.3 GHz, and they present a CA difference of 85°. Additionally, the combinations of the mode J_1 and higher modes J_3 and J_4 have the same MS at frequencies of 4.6 GHz and 5.6 GHz. The MS of 0.77 and 0.7 corresponds to the CA difference of 78° and 90°, respectively. It should be noted that when the ascending curve of one MS crosses with the descending curve of another MS at a point of 0.7, the corresponding CA difference is just 90°. In this way, whether the CA difference between two modes is close to 90° can be preliminarily determined. Besides, higher-order modes have maximum modal significance at much higher frequencies.

Figure 4 depicts the modal currents and radiation patterns of the three combinations of modes with the same amplitude and nearly 90° CA difference. As observed, at 3.3 GHz, J_1 and J_2 are characterized with vertical and horizontal currents (denoted by the blue arrow), respectively, and their directivity is consistent in the direction of the Z-axis. Thus, if these two modes are properly excited and combined, they would radiate CP waves within this frequency band.

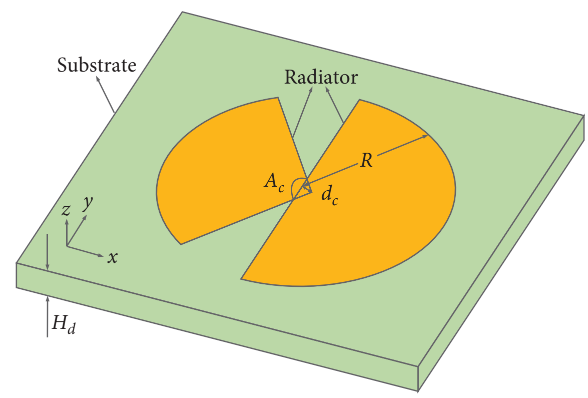

Figure 2: Geometry of the radiator. Dimensions: $R = 15$ mm, $A_c = 110°$, $d_c = 1.2$ mm, and $H_d = 1.6$ mm.

When the frequency rises to 4.6 GHz, although modes J_1 and J_3 have CP radiation potential only from the perspective of MS and CA, they actually contribute nothing to CP radiation due to their nonorthogonal current distribution, which can be seen clearly in Figure 4(b). As mode J_1 encounters mode J_4 at 5.6 GHz, J_4 is still able to radiate as expected in z-direction, but J_1 leads to a null gain in the far-field region of this direction. That's because the current distribution of J_1 in the vertical direction is opposite at two sides of the radiator. Thus, they cancel each other near the center. Although this combination deteriorates the radiation in the z-direction to a certain extent, it increases CP operation bandwidth. That is the price of getting wide ARBW without changing the structure. In a word, the radiator has the potential to perform CP radiation over 3.3 GHz–5.6 GHz.

3.2. Placement of Feed. Characteristic modes can be computed in the absence of a stimulus source. Once the information based on CMA is collected, the next step is to decide how to feed the radiator properly so that the desired modes are excited while the undesired modes are suppressed. For CP antenna designs, the excitation should be set

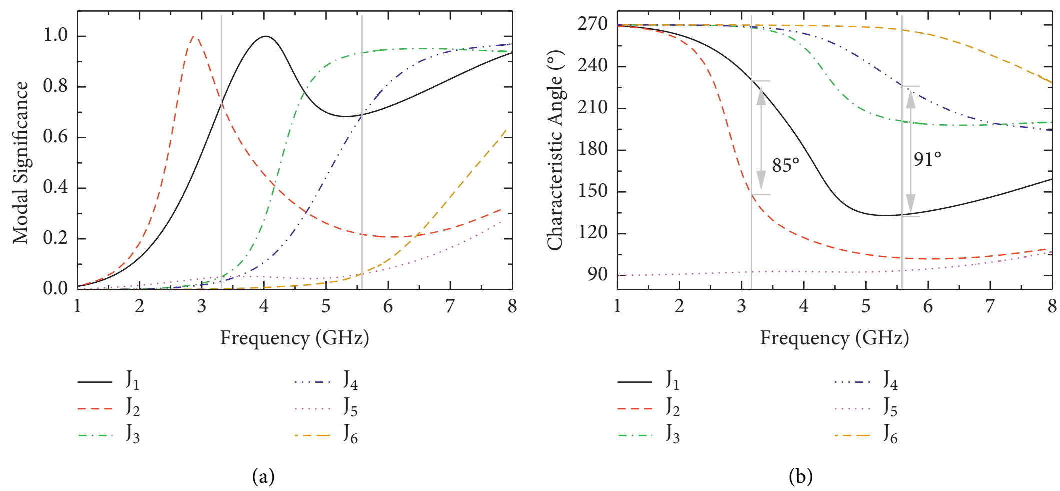

FIGURE 3: (a) Modal significance and (b) characteristic angle for the first six modes of radiator calculated at 4 GHz.

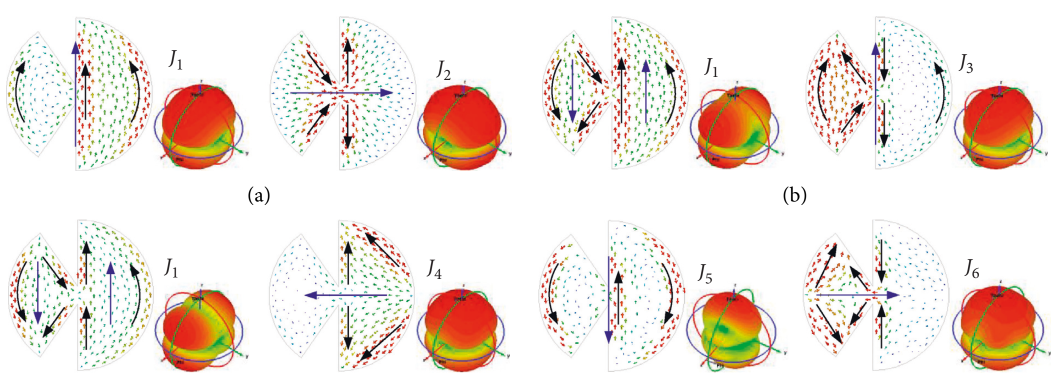

FIGURE 4: Modal currents and radiation patterns for the radiator of (a) modes J_1 and J_2 at 3.3 GHz. (b) Modes J_1 and J_3 at 4.6 GHz. (c) Modes J_1 and J_4 at 5.6 GHz. (d) Modes J_5 and J_6 at 7 GHz.

at the minimum difference between the operating modal currents due to the requirement of the same amplitude for the combined modes [17].

The position with a minimum difference value can be identified by subtracting the two modes that need to be excited, which can be done by "Mix 3D Fields" in CST. Figure 5 plots the current difference distribution of $J_1 - J_2$ and $J_1 - J_4$ at the MS crossover frequency of 3.3 GHz and 5.6 GHz, respectively. It is interesting to note that the minimum current regions of the two combinations occur on one arm of the semicircle, which is marked by Z_1 and Z_2 in Figure 5. Determining the exact type of excitation requires photographing the position of Z_1 and Z_2 into the corresponding modal current distribution, e.g., Figures 4(a) and 4(c). Clearly, both J_1 and J_2 have dense currents along the upper arm of the semicircle in the region of Z_1. While the region of Z_2 is photographed in Figure 4(c), the maximum current of J_1 and J_4 does not locate in this zone. However, upon further inspection, J_1 and J_4 in region Z_2 also have considerable current with similar intensity. Therefore, a current excitation is required in both cases, which can be achieved by a direct-feed or an inductive coupling feed technology [19]. Besides, Figure 4(d) reveals that J_5 and J_6 can also be activated if they have sufficient MS. It will happen when the feed line is introduced, which will be employed in the incoming distribution.

Then two prototypes of the antenna with different feeding mechanisms were designed, as shown in Figure 6 and CMA was performed again, which are named Proto A and Proto B, respectively. An explanation of the analysis process is needed here. The CMA for Proto A and Proto B analyzes the influence of the signal line on the radiator. Then, no matter what kind of ground plane is used, such as microstrip, CPW, or other deformations, it is necessary to include the signal line to constitute the feed, which is removed from the CMA and replaced by full-wave simulation for the convenience of design and optimization. The optimized dimensions of the prototypes are proposed in Table 1.

3.3. CMA of Proto A. Proto A is fabricated on a 1.6 mm thick FR-4 substrate with the dimension of $L_d \times W_d$ in Figure 6(a). A signal line with the length of L_1 and width of W_1 is connected to the radiator by a right triangular patch directly.

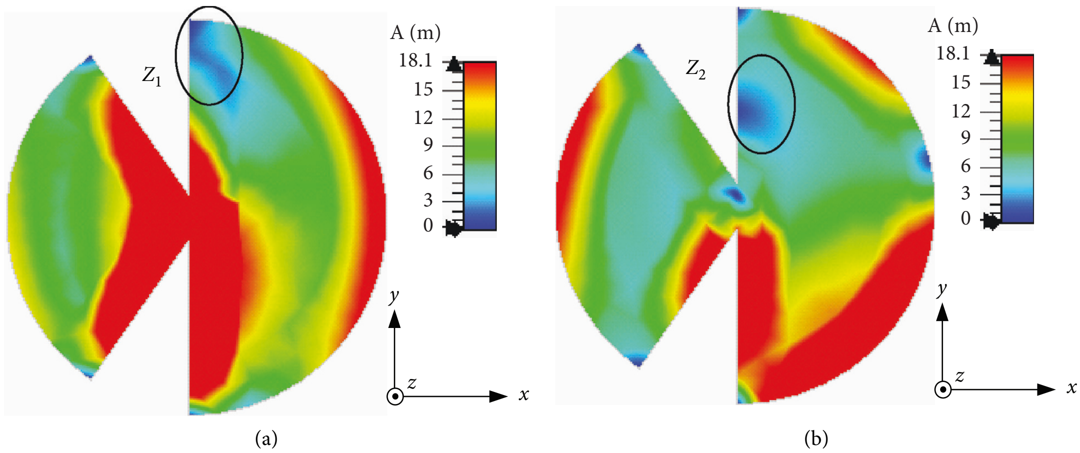

Figure 5: Current difference distribution between (a) J_1 and J_2 at 3.3 GHz; (b) J_1 and J_4 at 5.6 GHz.

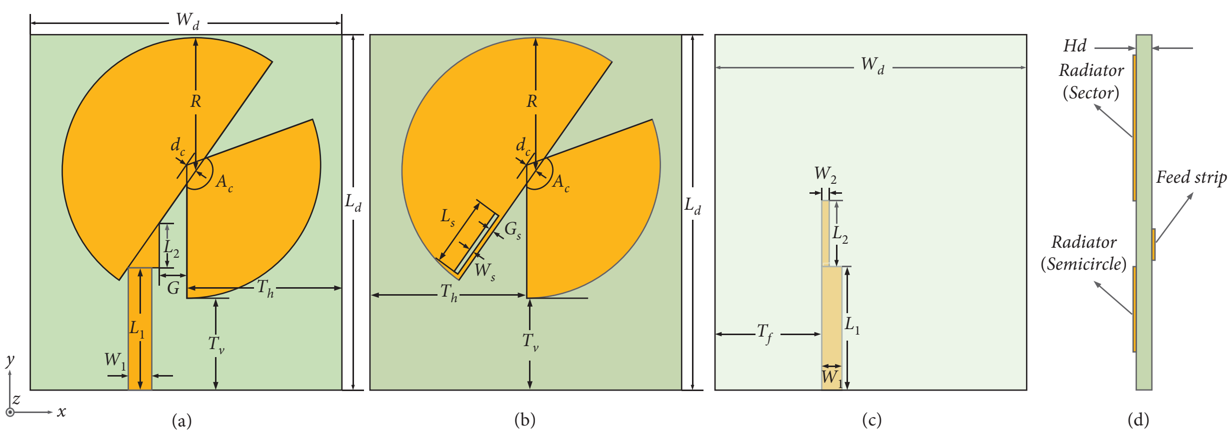

Figure 6: (a) Geometry of Proto A. (b) Top view of Proto B. (c) Perspective view of Proto B. (d) Side view of Proto B.

Table 1: Dimensions of Proto A and Proto B (unit: mm).

Proto A	R	A_c	d_c	L_d	W_d	L_1	W_1	L_2	T_v	T_h	G
Value	15	110°	1.2	40	35	13.4	2.6	5	10.4	15.4	3.1
Proto B	L_s	W_s	G_s	T_v	T_h	L_1	W_1	L_2	W_2	T_f	H_d
Value	8	0.5	0.5	10.4	17.6	13.9	2.3	5.5	0.8	12	1.6

The radiator is rotated 145° counterclockwise for convenience of feed placement. The hypotenuse is attached to the arm of the semicircle, and the side parallel to the sector has a length L_2. Once again, CMA is employed for analyzing and optimizing Proto A, with MS and CA plotted in Figure 7.

Comparing the modes depicted in Figures 3 and 7, it is clear that in addition to analyzing two more modes than before, the curves of dominant modes have changed significantly. All modes of Proto A resonate at higher frequencies than those of radiator except for mode J_o at around 2.4 GHz. Thus it can be inferred that J_o is introduced by the feed line. Meanwhile, it makes sense that modes J_{o1}, J_{o2}, J_{o3}, J_{o4}, J_{o5}, and J_{o6} of Proto A correspond to modes J_1, J_2, J_3, J_4, J_5, and J_6 of the radiator, respectively. This inference can be further confirmed by the modal currents and characteristic fields in the following analysis. The mode index "oN" (N is 1, 2, 3, . . ., etc.) is assigned to ensure consistency with the one of the radiator.

It should be noticed that J_{o1} no longer plays the role of "link mode," which combines J_{o2} and J_{o4}, respectively, to contribute to the upper and lower sideband of the CP radiation for the radiator. Instead, J_{o2} replaces J_{o1} as the link mode due to its gradual variation either after the resonance or intersection with J_{o1} in Proto A. In other words, it has the capacity to broaden the CP bandwidth when the intersection with the higher order mode occurs around 0.7 of MS. As portrayed in Figure 7, J_{o2} combines J_{o1}, J_{o3}, J_{o4}, and J_{o6} to feature CP potential at 4.3 GHz, 4.5 GHz, 6.1 GHz, and 7.1 GHz, respectively, if their equivalent currents are perpendicular to each other. Although J_o has the same MS as J_{o2} at 2.6 GHz, it is out of consideration due to the uncertainty of whether the mode can be activated by the feed structure.

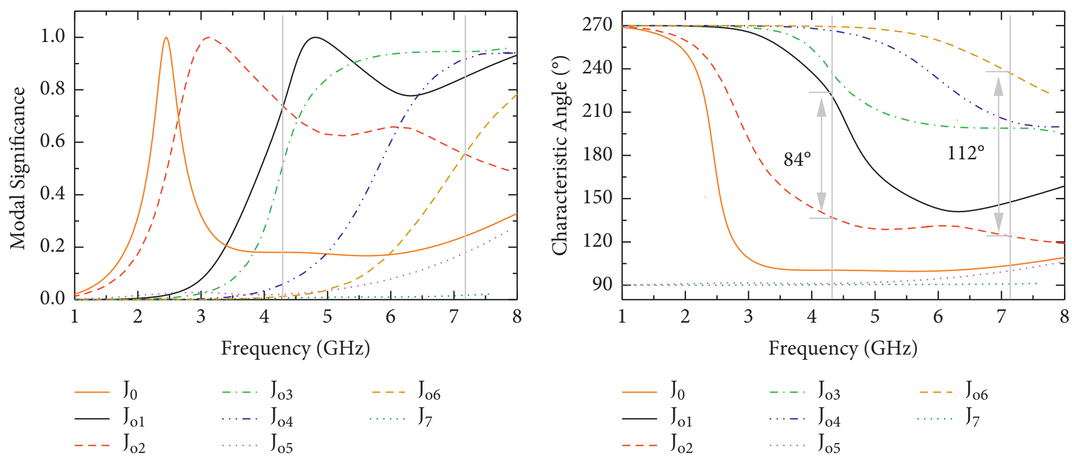

(a) (b)

FIGURE 7: (a) Modal significance and (b) Characteristic angle for the first eight modes of Proto A calculated at 4 GHz.

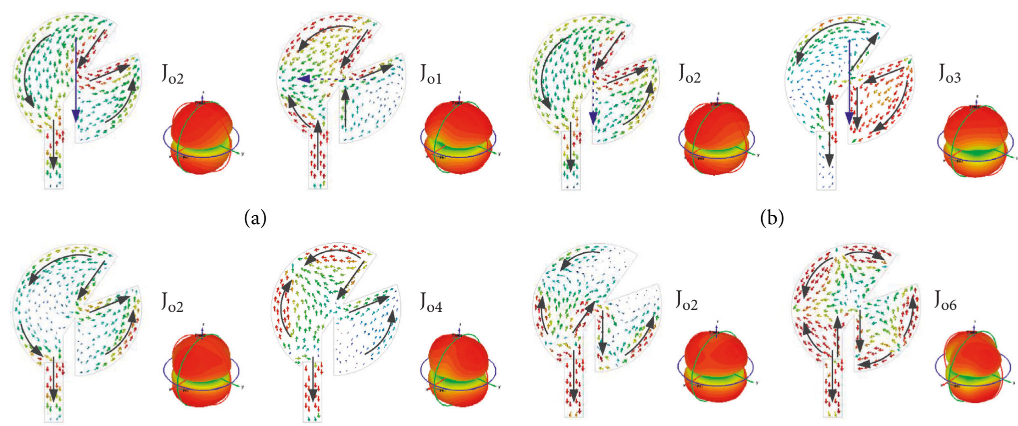

(a) (b) (c) (d)

FIGURE 8: Modal currents and radiation patterns for the Proto A of (a) modes J_{o1} and J_{o2} at 4.3 GHz. (b) Modes J_{o2} and J_{o3} at 4.5 GHz. (c) Modes J_{o2} and J_{o4} at 6.1 GHz. (d) Modes J_{o2} and J_{o6} at 7.1 GHz.

That can be verified by the final result. Otherwise, the existing feed needs to be considered as a part of the radiator, and then the design goes back to the feed design stage (Subsection 3.2). It is an endless loop until the designer interrupts it, which makes the design complicated and weird. Combined with the CA in Figure 7(b), the potential of these modes featuring CP radiation needs to be further validated by the modal current.

Figure 8 depicts the modal currents and radiation patterns for the modes of interest. The total current is denoted by a blue arrow where the solid line indicates that the far-field corresponding to the current radiates in the z-direction, and the dotted line indicates that the radiation along the z-direction has slightly worsened. Without the blue arrow, the gain in z-direction radiates very little or is even null due to the cancellation of the current at the center. As observed, the current distribution that feature CP radiation gets messy. However, comparing the current in Figures 4 and 8, it can be concluded that the current distribution of these corresponding modes is roughly similar. For example, the currents of J_1 and J_{o1} are mainly distributed in the semi-circular radiator. The same goes for the other modes in Figure 8. Hence, the previous inference about the mode tracking is further confirmed.

It is worth mentioning that all CP modes do not have a strict perpendicularity in terms of current distribution after the introduction of the signal line. The blue arrow is only an approximation of the equivalent total current. However, CP radiation can also be produced by the CP modes with sufficient angle under the criterion of 3dB-AR. In addition, in the next step of antenna design, the angle between the CP modes can be improved by tuning the ground plane size to make it close to the requirement of perpendicular current distribution. The far fields in Figure 8 also reveal the phenomenon that multiple modes are involved in a frequency band. The gain deteriorates and even radiates null in the z-direction. J_{o2} acts as a link mode across the band of interest. Thus, its gain deterioration inevitably causes the directivity of the antenna based on Proto A to deviate from the z-axis in high frequency band.

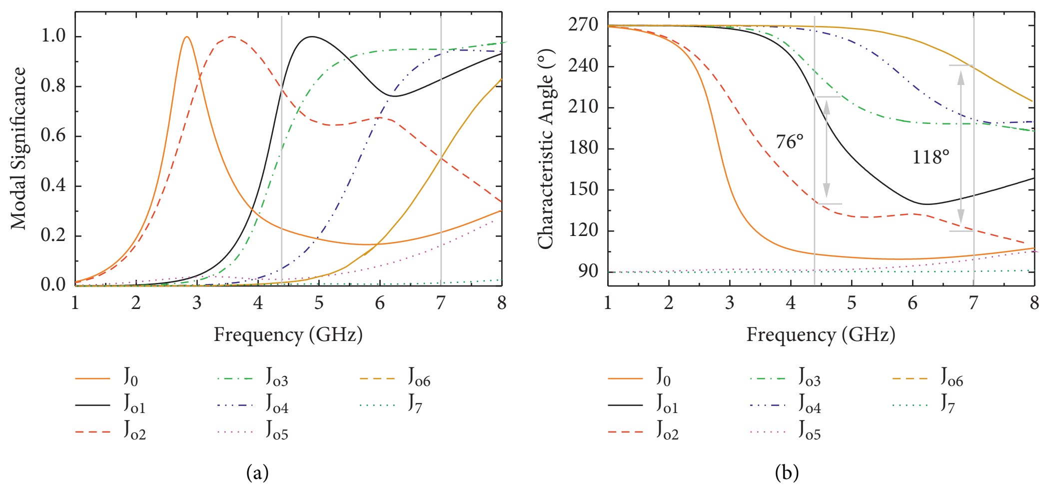

Figure 9: (a) Modal significance and (b) characteristic angle for the first eight modes of Proto B calculated at 4 GHz.

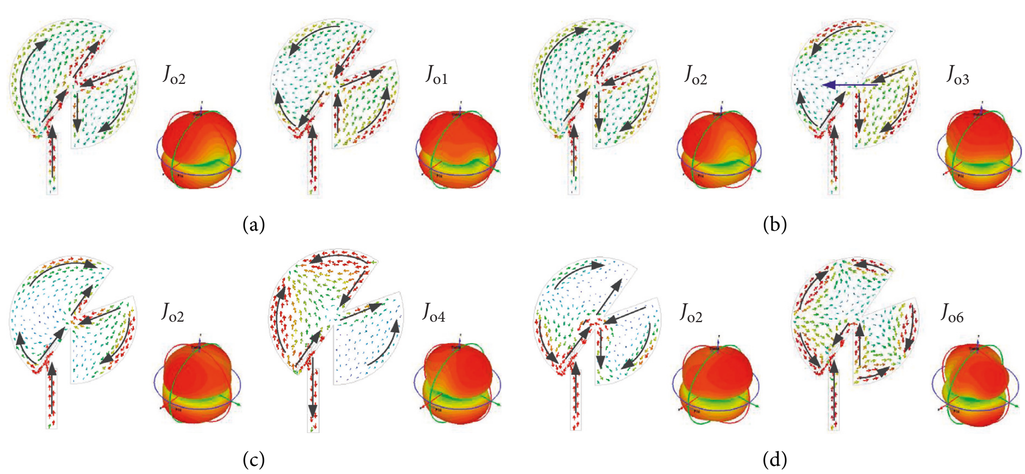

Figure 10: Modal currents and radiation patterns for Proto B of (a) modes J_{o1} and J_{o2} at 4.4 GHz. (b) Modes J_{o2} and J_{o3} at 4.6 GHz. (c) Modes J_{o2} and J_{o4} at 6 GHz. (d) Modes J_{o2} and J_{o6} at 7 GHz.

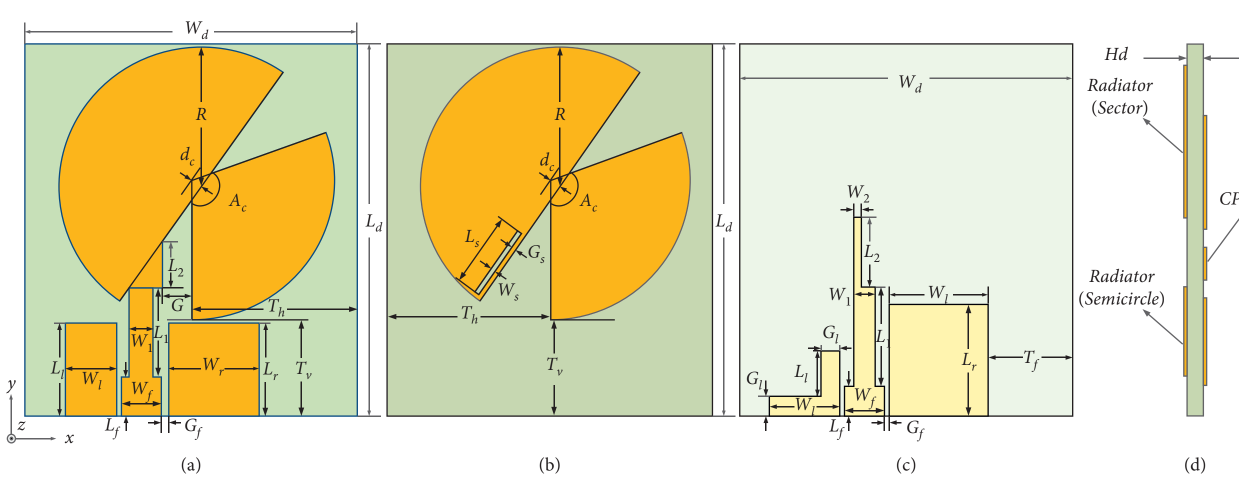

Figure 11: (a) Geometry of An1. (b) Top view of An2. (c) Perspective of An2. (d) Side view of An2.

Table 2: Dimensions of the proposed antennas (unit: mm).

An1	L_f	W_f	L_1	W_1	L_2	G	T_v	T_h	L_l	L_r	W_l	W_r	G_f
Value	4.2	4.2	9.6	2.6	5	3.1	10.4	20.2	10	10	5.4	9.8	0.5
An2	L_1	W_1	L_2	W_2	L_f	W_f	G_f	W_l	L_l	G_l	W_r	L_r	T_f
Value	10.7	2.3	7.5	0.8	3.2	4.2	0.5	7.4	5.5	1.5	10.4	12	8.9

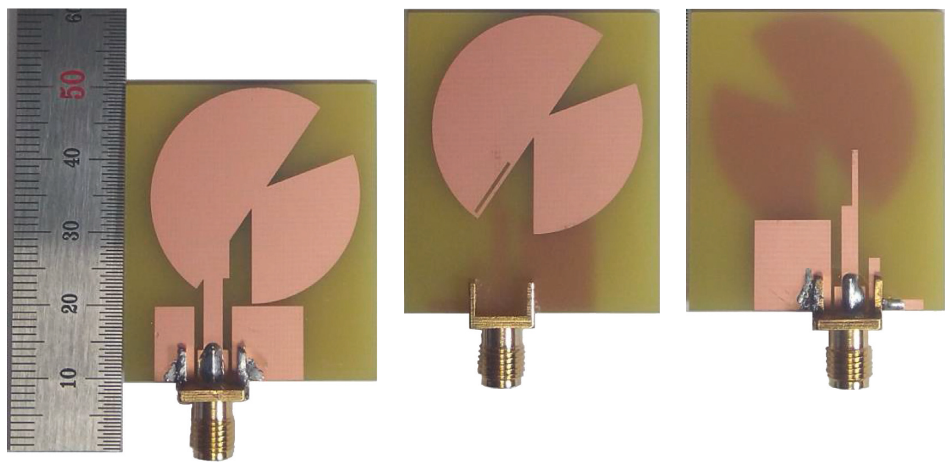

(a) (b) (c)

Figure 12: (a) Fabricated An1. (b) The top view of fabricated An2. (c) The back view of fabricated An2.

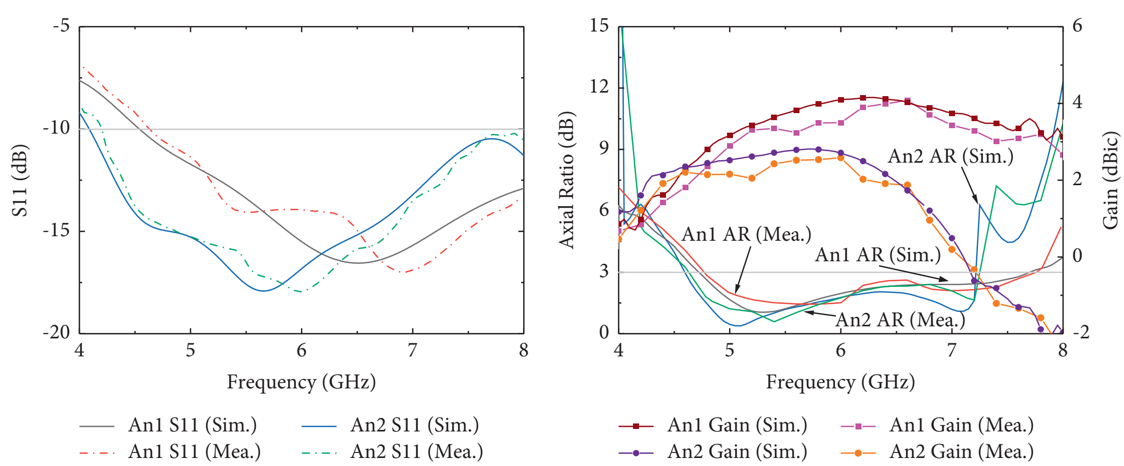

(a) (b)

Figure 13: Simulated and measured (a) S11. (b) AR and gain.

Based on the above analysis, it is reasonable to expect that J_{o1}, J_{o2}, J_{o3}, $J_{o4,}$ and J_{o6} can be excited through the feed mechanism. The other modes are ignored due to no contribution to CP radiation in the operating band. Thus Proto A has the CP potential over 4.3 GHz–7.1 GHz.

3.4. CMA of Proto B. Proto B has the same substrate as Proto A. To achieve the inductive coupling feed [19], a slit ($W_s \times L_s$) is etched on the edge of the semicircle with a distance of $G_{s,}$ as shown in Figure 6(b). The slit is so narrow and close to the edge that it has little effect on the current distribution of the original radiator. A stepped-impedance feeding patch is printed on the other side of the substrate relative to the radiator, which consists of a $W_1 \times L_1$ strip and a $W_2 \times L_2$ strip displayed in Figure 6(c).

Figure 9 portrays the MS and CA for the first eight modes. As the analysis for Proto A, the modes are tracked and reindexed, i.e., modes J_{o1}, J_{o2}, J_{o3}, J_{o4}, $J_{o5,}$ and J_{o6} of Proto B correspond to modes J_1, J_2, J_3, J_4, $J_{5,}$ and J_6 of the radiator,

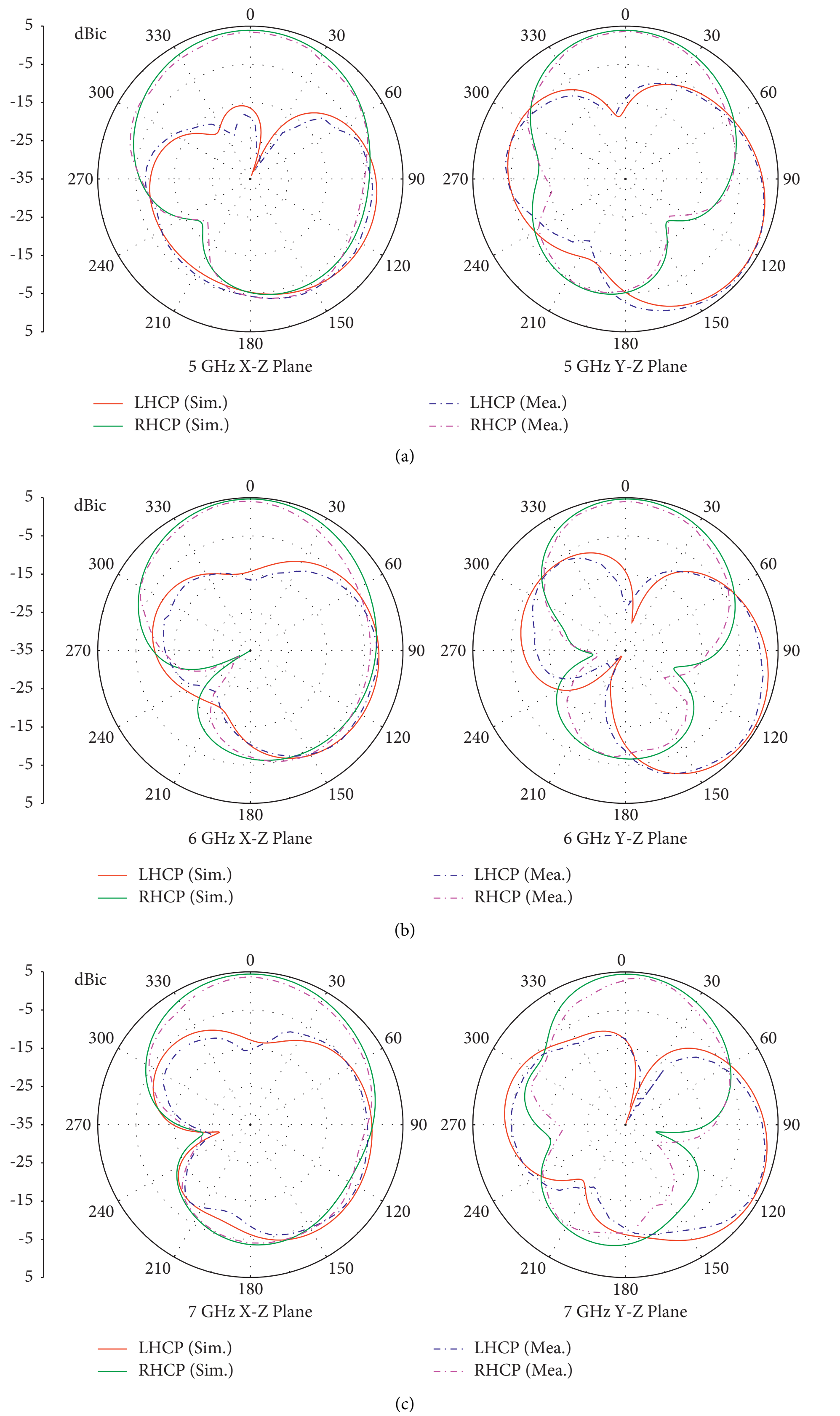

Figure 14: Simulated and measured radiation patterns of An1 at (a) 5 GHz, (b) 6 GHz, and (c) 7 GHz.

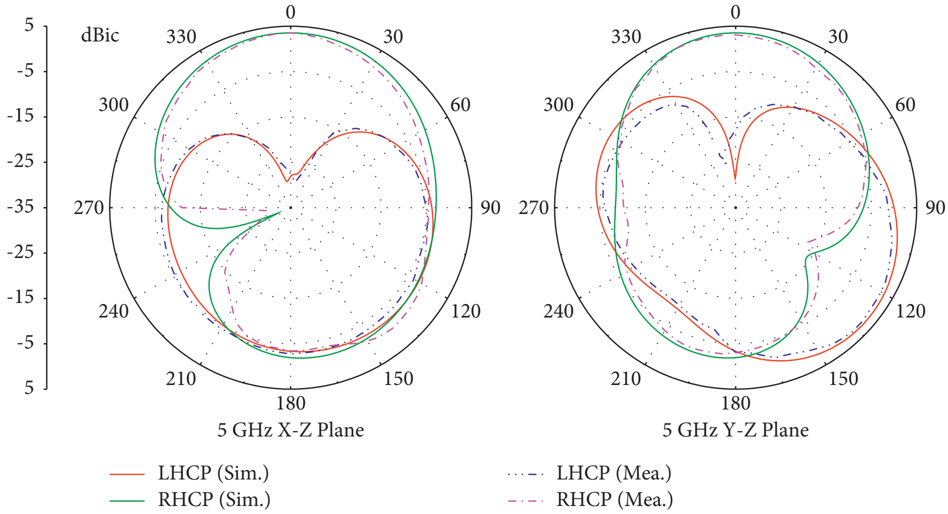

(a)

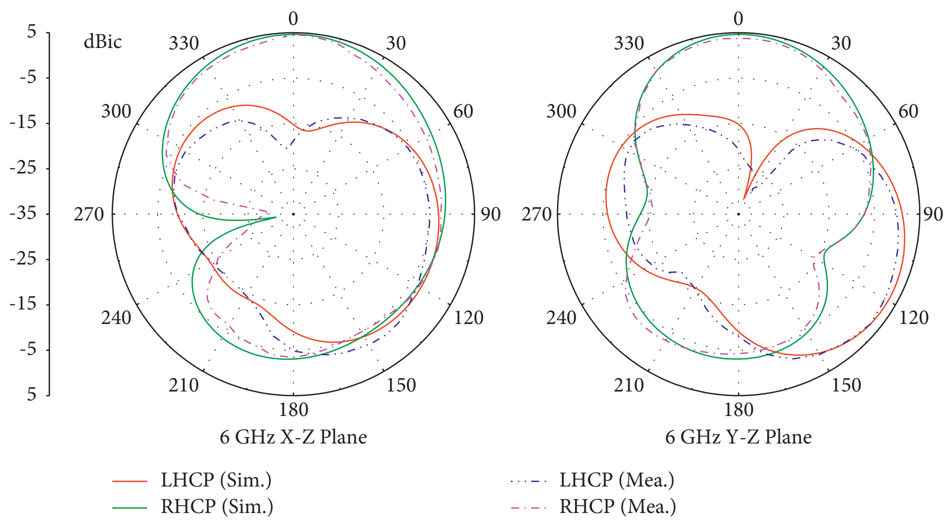

(b)

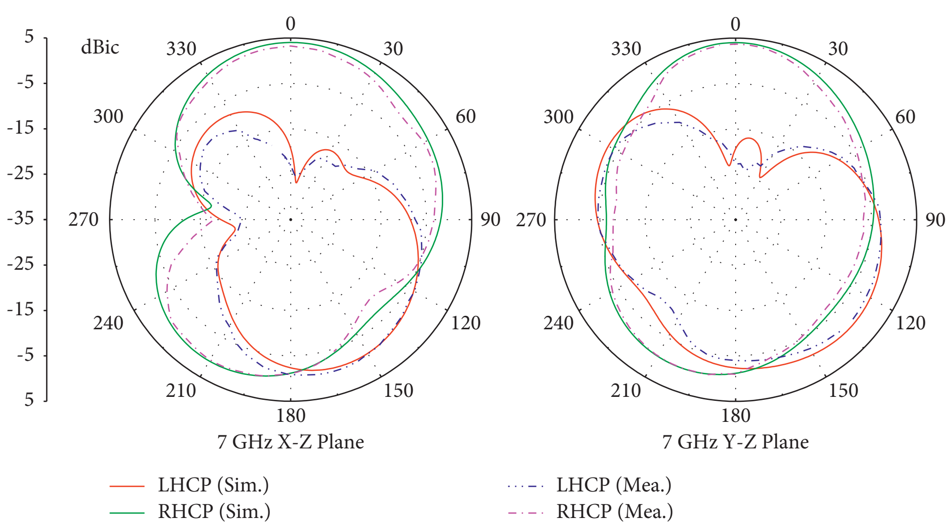

(c)

Figure 15: Simulated and measured radiation patterns of An2 at (a) 5 GHz, (b) 6 GHz, and (c) 7 GHz.

Table 3: Comparison between An1 and An2.

Prop. An.	Feeding mechanism	CPBW by CMA (GHz)	3 dB ARBW (GHz)	Max gain (dBic)	Min gain (dBic)
An1	Direct feed	4.3–7.1	4.7–7.7	4.0	2.4
An2	Inductive coupler	4.4–7.0	4.6–7.2	2.5	−0.4

Table 4: Comparisons of the proposed and other CP antennas.

Ref.	Dimensions ($\lambda_0 \times \lambda_0 \times \lambda_0$)	3-dB AR bandwidth	Peak gain (dBic)
[4]	0.48 × 0.48 × 0.006	28.8% (2.06–2.76 GHz)	4.0
[5]	0.33 × 0.45 × 0.02	42.6% (4.80–7.40 GHz)	2.3
[6]	1.42 × 2.24 × 0.034	74.3% (4.18–9.12 GHz)	7.3
[22]	0.54 × 0.54 × 0.019	91.0% (2.10–5.60 GHz)	3.2
[23]	0.28 × 0.36 × 0.017	43.4% (2.40–3.73 GHz)	3.8
Prop.An1	0.72 × 0.83 × 0.033	48.3% (4.70–7.70 GHz)	4.0
Prop.An2	0.69 × 0.79 × 0.031	44.0% (4.6–7.20 GHz)	2.5

AR bandwidth: AR < 3 dB; λ_0: free-space wavelength at the center frequency of the 3-dB AR bandwidth.

respectively. It is observed that the characteristics of these modes are so similar in both prototypes, with only slight differences in resonance frequencies.

Figure 10 illustrates the modal current and characteristic field for the modes of concern. Similar to Proto A, not all CP modes for Proto B exhibit the characteristic of current with strict perpendicularity. It is worth mentioning that of all the modes, only J_{o3} radiates along the z-direction. As shown in Figure 4(b), J_{o3} can also be excited by the feed. Compared with the direct feed, the inductive coupling feed has a greater effect on the current distribution of the radiator. As in the case of Proto A, the gain in z-direction deteriorates with increasing frequency. In a word, together with the information provided by CA in Figure 9(b), the potential for CP radiation can be achieved over 4.4 GHz–7 GHz.

4. Experimental Verification

To verify the effectiveness of CMA for CP antenna design, An1 and An2 based on Proto A and Proto B are proposed, respectively, as shown in Figure 11. For the sake of comparison, both antennas are fed by 50 Ω coplanar waveguide (CPW) with a signal line of width $W_f = 4.2$ mm and two identical gaps of width $G_f = 0.5$ mm between the signal line and the coplanar ground plane. The CPW employed by An1 has two rectangular patches as coplanar ground with equal height and unequal width, while the CPW used by An2 consists of an inverted L-shaped patch and a rectangular ground. The initial geometrical parameters of the antennas are determined by CMA in Section 3. In order to improve antenna performance, full-wave simulation with radiation boundary is performed, and the final optimized geometrical parameters are shown in Table 2. Then, the proposed antennas are fabricated and characterized to verify the design procedure and their photos are presented in Figure 12.

Figure 13 illustrates the simulated and measured S11, AR, and gain for An1 and An2. A good agreement between the simulated and measured results can be observed. An1 is able to achieve good CP performance in the wide range of frequency bands from 4.7 to 7.7 GHz, equivalent to 48.3% ARBW. The measured realized gain within the CP operating band is varied from 2.4 to 4.0 dBic. Compared with the information provided by the CMA, the introduction of the CPW ground plane leads to the CP modes shifting to a higher frequency, similar to the signal line analyzed previously. Additionally, a wider ARBW is obtained, which is due to the CPW ground plane improving the MS of the mode J_{o5} in the upper band so that J_{o5} can intersect with the link mode J_{o2} to contribute CP radiation and broaden ARBW. In observation of An2, the measured CP bandwidth is 44% (4.6 GHz–7.2 GHz), and a maximum realized gain of 2.5 dBic is obtained at around 5.8 GHz. Unfortunately, the gain drops sharply in the upper band, reaching a minimum of −0.4 dBic at 7.2 GHz.

The simulated and measured radiation patterns in both of X-Z Plane and Y-Z Plane at 5 GHz, 6 GHz, and 7 GHz for An1 and An2 are plotted in Figures 14 and 15, respectively. For both antennas, basically, the agreement between simulations and measurements is observed with the sense of polarization, i.e., RHCP in the +z-direction.

It can be seen from the radiation patterns that the LHCP of the two antennas deviates in the-z-direction. Without CMA, a resulting conclusion of asymmetric structure may be used to illustrate the problem simply. However, the explanation from the perspective of CMA provides more theoretical evidence and guiding significance: with the increase of frequency, the link mode J_{o2} encounters more modes of interference, and its radiation tends to be null in the z-direction, resulting in a more serious deviation of LHCP from z-direction. This deviation has been inferred in the CMA analysis previously, which is the advantage of CMA—obtaining the information about antenna radiation from the beginning of design in the absence of excitation.

Table 3 compares An1 with An2 in terms of feeding mechanism, 3 dB ARBW, maximum gain, minimum gain, and CP bandwidth(CPBW) provided by CMA. As can be seen, An1 possesses greater bandwidth and gain with higher flatness in the operating band. However, An2 reveals a higher consistency with the information provided by CMA in terms of ARBW. It can be seen a well-designed feed can contribute better CP performance to the same radiator.

Table 4 summarizes some key indicators of the proposed antenna and other wideband CP antennas. Apparently, there is a trade-off among lateral sizes, ARBW, and peak gain. The data indicate that the proposed antennas (An1 and An2) exhibit a middle value of ARBW and electrical size in the reference antennas. Although the designs in [6, 22] show a wider ARBW, they exhibit larger electrical sizes and lower gain, respectively, relative to the proposed An1. The characteristics of An2 with low gain and poor flatness over the CP operation band limit its application. Overall, the antennas show comparable performance in terms of dimension, impedance bandwidth, AR bandwidth, and process complexity.

5. Conclusion

A design procedure using characteristic mode analysis has been used to design two circular polarized microstrip patch antennas consisting of the same radiator fed by different feed structures. In this paper, a complete process for designing a circularly polarized antenna based on CMA is proposed and implemented, including modal current and radiation field analysis, mode selection, feed design, and antenna full wave simulation, which provides a better insight into the principle of circularly polarized antennas. The design method of the CP antenna can be extended to other types of structures with clear theoretical explanations and directional guidance for optimization.

Because of the orthogonality of modal currents, CMA has natural advantages in designing CP antenna compared with other approaches. Through the design procedure above, the radiator and feed are designed separately, which provides great convenience for the design of CP antenna. Moreover, Proto A (B) builds a bridge from the radiator to the final antenna, providing considerable CP radiation information, which can predict the CP performance in the absence of excitation. Thus, evidence of the feasibility of the design can be obtained to guide the design for the next step. The final simulated and experimental results are in good agreement with the prediction based on CMA verify the procedure.

Data Availability

The data used to support the findings of this study are included within the article.

Conflicts of Interest

The authors declare that they have no conflicts of interest.

Acknowledgments

This work was supported by the National Natural Science Foundation of China General Program under Grant 61971210 and the Youth project of Liaoning Provincial Department of Education under Grant LJ2019QL024.

References

[1] M. Ali, A. T. M. Sayem, and V. K. Kunda, "A rsmicrostrip patch antenna for satellite and terrestrial links," *IEEE Transactions on Vehicular Technology*, vol. 56, no. 2, pp. 426–435, 2007.

[2] Y. Cao, S. W. Cheung, and T. I. Yuk, "A simple planar polarization reconfigurable monopole antenna for GNSS/PCS," *IEEE Transactions on Antennas and Propagation*, vol. 63, no. 2, pp. 500–507, 2015.

[3] H. D. Horng-Dean Chen, "Broadband CPW-fed square slot antennas with a widened tuning stub," *IEEE Transactions on Antennas and Propagation*, vol. 51, no. 8, pp. 1982–1986, 2003.

[4] J. Y. Chi-Chaan Chang and C. C. Chang, "Circularly polarized square slot antenna with a pair of inverted-L grounded strips," *IEEE Antennas and Wireless Propagation Letters*, vol. 7, pp. 149–151, 2008.

[5] K. O. Gyasi, J. G. Wen, D. Inserra, Y. Huang, and H. Zhang, "A compact broadband cross-shaped circularly polarized planar monopole antenna with a ground plane extension," *IEEE Antennas and Wireless Propagation Letters*, vol. 17, no. 99, p. 1, 2018.

[6] T. T. Le, H. T. Huy, and H. C. Park, "Simple-structured dual-slot broadband circularly polarized antenna," *IEEE Antennas and Wireless Propagation Letters*, vol. 17, p. 1, 2018.

[7] H. Zhang, Y. C. Jiao, L. Liang, and Z. Chi, "Broadband circularly polarized square-ring-loaded slot antenna with flat gains," *IEEE Antennas and Wireless Propagation Letters*, vol. 16, no. 99, pp. 29–32, 2016.

[8] C. Ds and S. S. Karthikeyan, "A novel broadband dual circularly polarized microstrip-fed monopole antenna," *IEEE Transactions on Antennas and Propagation*, vol. 3, p. 1, 2017.

[9] K. Ding, C. Gao, T. Yu, D. Qu, and B. Zhang, "Gainimproved broadband circularly polarized antenna array with parasitic patches," *IEEE Antennas and Wireless Propagation Letters*, vol. 16, pp. 1468–1471, 2017.

[10] M. Cabedo-Fabres, E. Antonino-Daviu, A. Valero-Nogueira, and M. Bataller, "The theory of characteristic modes revisited: a contribution to the design of antennas for modern applications," *IEEE Antennas and Propagation Magazine*, vol. 49, no. 5, pp. 52–68, 2007.

[11] J. F. Lin and L. Zhu, "Low-profile high-directivity circularly-polarized differential-fed patch antenna with characteristic modes analysis," *IEEE Transactions on Antennas and Propagation*, vol. 99, p. 1, 2020.

[12] P. W. Futter and U. Jakobus, "Antenna positioning for bandwidth optimization using characteristic mode analysis," in *Proceedings of the 2020 14th European Conference on Antennas and Propagation (EuCAP)*, Copenhagen, Denmark, March 2020.

[13] J. R. Garbacz, "Modal expansions for resonance scattering phenomena," *Proceedings of the IEEE*, vol. 53, no. 8, pp. 856–864, 1965.

[14] R. Harrington and J. Mautz, "Theory of characteristic modes for conducting bodies," *IEEE Transactions on Antennas and Propagation*, vol. 19, no. 5, pp. 622–628, 1971.

[15] W. Li, Y. Liu, J. Li, L. Ye, and Q. H. Liu, "Modal proportion analysis in antenna characteristic mode theory," *International Journal of Antennas and Propagation*, vol. 2019, pp. 1–10, 2019.

[16] H. Shaode, P. Jin, and L. Yuyue, "Study on the relationships between eigenmodes, natural modes, and characteristic modes of perfectly electric conducting bodies," *International*

Journal of Antennas and Propagation, vol. 2018, pp. 1–13, 2018.

[17] Y. Chao-Fu Wang and C. F. Wang, “Characteristic-mode-based improvement of circularly polarized U-slot and E-shaped patch antennas,” *IEEE Antennas and Wireless Propagation Letters*, vol. 11, pp. 1474–1477, 2012.

[18] B. B. Q. Elias, P. J. Soh, A. A. Al-Hadi, and P. Akkaraekthalin, “Gain optimization of low-profile textile antennas using CMA and active mode subtraction method,” *IEEE Access*, vol. 9, pp. 23691–23704, 2021.

[19] R. Martens and D. Manteuffel, “A feed network for the selective excitation of specific characteristic modes on small terminals,” in *Proceedings of the European Conference on Antennas and Propagation*, pp. 1842–1846, Prague, Czech Republic, March 2012.

[20] W. Xu, J. Nan, and M. Gao, “Compact broadband circularly polarized CPW-Fed antenna with characteristic mode analysis,” *International Journal of Antennas and Propagation*, vol. 2022, Article ID 9002700, 11 pages, 2022.

[21] J. Ethier, E. Lanoue, and D. McNamara, “MIMO handheld antenna design approach using characteristic mode concepts,” *Microwave and Optical Technology Letters*, vol. 50, no. 7, pp. 1724–1727, 2008.

[22] H. H. Tran, N. Nguyen-Trong, and A. M. Abbosh, “Simple design procedure of a broadband circularly polarized slot monopole antenna assisted by characteristic mode analysis,” *IEEE Access*, vol. 6, p. 1, 2018.

[23] M. Han and W. Dou, “Compact clock-shaped broadband circularly polarized antenna based on characteristic mode analysis,” *IEEE Access*, vol. 99, p. 1, 2019.